Published for SISSA by Springer

Received: July 15, 2022
Accepted: October 6, 2022
Published: October 17, 2022

Probing non-standard $HVV(V = W, Z)$ couplings in single Higgs production at future electron-proton collider

Pramod Sharma and Ambresh Shivaji

Indian Institute of Science Education and Research, Knowledge City, Sector 81, S.A.S. Nagar, Manauli PO 140306, Punjab, India

E-mail: pramodsharma.iiser@gmail.com, ashivaji@iisermohali.ac.in

Abstract: The couplings of the Higgs boson (H) with massive gauge bosons of weak interaction ($V = W, Z$), can be probed in single Higgs boson production at the proposed future Large Hadron-Electron Collider (LHeC). In the collision of an electron with a proton, single Higgs production takes place via so-called charged-current ($e^- p \to \nu_e H j$) and neutral-current ($e^- p \to e^- H j$) processes. We explore the potential of the azimuthal angle correlation between the forward jet and scattered neutrino or electron in probing the non-standard HVV couplings at the collider center-of-mass energy of $\sqrt{s} \approx 1.3\,\text{TeV}$. We choose the most general modifications (of CP-even and CP-odd nature) to these couplings due to new physics effects beyond the standard model. We derive exclusion limits on new physics parameters of HVV couplings as a function of integrated luminosity at 95% C.L. using the azimuthal angular correlations in charged- and neutral-current processes. We find that using 1000 fb^{-1} data, the standard model-like new physics parameters in HWW and HZZ couplings can be constrained with accuracies of 4% and 15%, respectively. The least constrained CP-even parameters of HWW coupling can be as large as 0.04, while those of HZZ coupling can have values around 0.31. Allowed values of CP-odd parameters in HWW and HZZ couplings are found to be around 0.14 and 0.34, respectively. We also study changes in the allowed values of non-trivial new physics parameters in the presence of other parameters.

Keywords: Anomalous Higgs Couplings, Higgs Production, Higgs Properties

ArXiv ePrint: 2207.03862

https://doi.org/10.1007/JHEP10(2022)108

JHEP10(2022)108

Contents

1 Introduction

The minimal electroweak standard model of particle physics predicts the existence of a fundamental massive scalar particle, the Higgs boson [1–7]. The mass of the Higgs boson is not a prediction of the model. However, once its mass is measured, its couplings with other standard model particles can be determined. The ATLAS and CMS experiments at the Large hadron Collider (LHC) have confirmed the discovery of a scalar particle of mass 125 GeV which is very much like the standard model Higgs boson [8–10]. The fact that no clear evidence of new physics has emerged in the entire gauge-Higgs sector, precise measurement of various couplings in the Higgs sector is one of the main goals of the future high energy collider projects [11]. In a scenario where high scale new physics effects in Higgs-vector boson couplings are parametrized by a common factor κ_V, the combined analyses of CMS and ATLAS taking the LHC Run-I data lead to $\kappa_V = 1.03 \pm 0.03$ [12, 13]. The expected accuracy on κ_V at the HL-LHC is below 2% [14]. It is well known that new physics effects may introduce new Lorentz structures and therefore new parameters in $HVV(V = W, Z)$ couplings [15].

The most general Lagrangian which can account for all possible three-point interactions involving Higgs and massive electroweak gauge bosons can be written as,

$$\begin{aligned}\mathcal{L}_{HVV}^{\rm BSM} = g\ &\left(m_V \kappa_W W_\mu^+ W^{-\mu} + \frac{\kappa_Z}{2\cos\theta_W} m_Z Z_\mu Z^\mu\right) H \\ &- \frac{g}{m_W}\left[\frac{\lambda_{1W}}{2} W^{+\mu\nu} W^-_{\mu\nu} + \frac{\lambda_{1Z}}{4} Z^{\mu\nu} Z_{\mu\nu} + \lambda_{2W}(W^{+\nu}\partial^\mu W^-_{\mu\nu} + h.c.) + \lambda_{2Z} Z^\nu \partial^\mu Z_{\mu\nu}\right. \\ &\left. + \frac{\tilde{\lambda}_W}{2} W^{+\mu\nu}\widetilde{W}^-_{\mu\nu} + \frac{\tilde{\lambda}_Z}{4} Z^{\mu\nu}\widetilde{Z}_{\mu\nu}\right] H, \end{aligned} \tag{1.1}$$

where g is the SU(2) coupling parameter and $\widetilde{V}^{\mu\nu} = \frac{1}{2}\epsilon^{\mu\nu\rho\sigma} V_{\rho\sigma}$ is the dual field strength tensor. The beyond the standard model (BSM) parameters κ_V and $\lambda_{iV}(i = 1, 2)$ are

JHEP10(2022)108

associated with CP-even, while $\tilde{\lambda}_V$ are associated with CP-odd couplings of the Higgs with vector bosons. The standard model (SM) predictions correspond to $\kappa_V = 1, \lambda_{iV} = 0 = \tilde{\lambda}_V$. The Lorentz structures of eq. (1.1) can be derived from the $\mathrm{SU}(2)_L \otimes \mathrm{U}(1)_Y$ gauge invariant dimension-6 operators [16–21]. The above framework is equivalent to the so-called Higgs basis [15]. The HVV vertex factor in our framework is given by,

$$\begin{aligned}\Gamma^{\mu\nu}_{HVV}(p_1,p_2) = g_V m_V \kappa_V g^{\mu\nu} + \frac{g}{m_W}\Big[&\lambda_{1V}(p_1^\nu p_2^\mu - g^{\mu\nu} p_1.p_2) \\ &+ \lambda_{2V}(p_1^\mu p_1^\nu + p_2^\mu p_2^\nu - g^{\mu\nu} p_1.p_1 - g^{\mu\nu} p_2.p_2) \\ &+ \widetilde{\lambda}_V\ \epsilon^{\mu\nu\alpha\beta} p_{1\alpha} p_{2\beta}\Big]. \end{aligned} \tag{1.2}$$

Here, p_1 (μ) and p_2 (ν) denote the momenta (Lorentz indices) of the two vector bosons in HVV coupling. Also, we have defined $g_W = g$ and $g_Z = g/\cos\theta_W$, θ_W being the Weinberg angle. Note that the parameter λ_{2V} is linked with the off-shellness of the vector bosons.

The new physics parametrization similar to the above one has been used to study HVV couplings at various current and future colliders [22–46]. Several studies exist in the literature which consider new physics effects in HVV couplings in an EFT framework via dimension-6 operators [47–69]. For a one-to-one correspondence between the two frameworks dictionaries like [35] can be used.

In this paper, we study the effect of the BSM parameters of HVV vertex in charged-current and neutral-current processes at the future Large Hadron Electron Collider (LHeC) [70, 71]. These processes have been studied in the context of Higgs boson searches in $H \to b\bar{b}$ decay mode [72]. The role of azimuthal angle between missing energy and jet in the transverse plane was investigated to distinguish CP-odd coupling from the CP-even coupling in the charged-current process [30]. In the present study, we have extended the theoretical framework considered in [30] which takes note of the fact that in charged-current and neutral-current processes the virtuality of mediating W and Z bosons changes event-by-event. This effect introduces one more CP-even parameter λ_{2V} in the analysis. We also study the neutral current process in detail using the azimuthal angle correlation between the final state e^- and the jet.

2 BSM effects in single Higgs production

At e^-p collider, the single Higgs production takes place via charged-current (CC) and neutral-current (NC) processes,

$$\begin{aligned} e^-p &\to \nu_e H j + X \qquad [\mathtt{CC}] \\ e^-p &\to e^- H j + X. \qquad [\mathtt{NC}] \end{aligned}$$

where j is a light quark jet (u, d, c, s). Leading order Feynman diagrams for these processes are shown in figure 1. The CC and NC processes are sensitive to HWW and HZZ couplings, respectively.[1] These processes are very similar to the vector boson fusion (VBF) processes

[1] Presence of $Hf\bar{f}'V$ contact interaction can also affect the predictions for CC and NC processes. However, using the equations of motion [73], such four-point interaction can be traded off for HVV interaction associated with λ_{2V} term in eq. (1.1).

JHEP10(2022)108

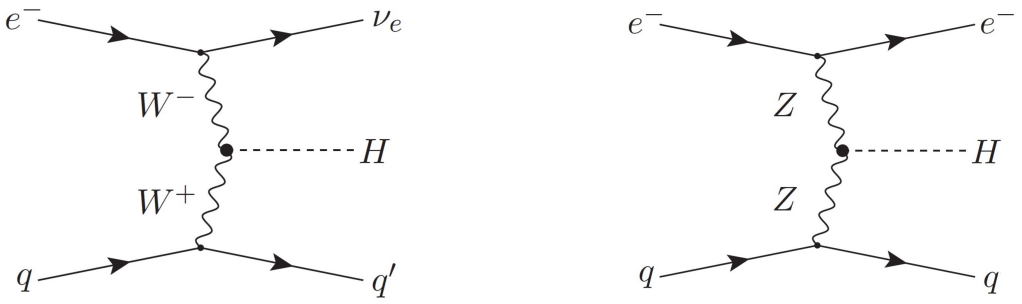

(a) **(b)**

Figure 1. Leading order Feynman diagrams for single Higgs production at e^-p collider. (a) Charged-current process. (b) Neutral-current process.

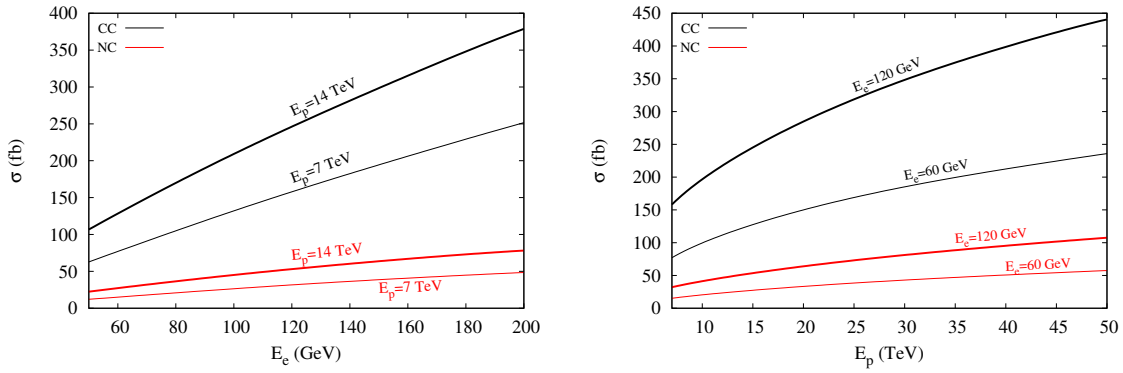

(a) **(b)**

Figure 2. Variation of `CC` (black) and `NC` (red) cross sections with respect to the electron beam energy, E_e (left), and proton beam energy, E_p (right).

$pp \to Hjj$ for Higgs production at the LHC. However, unlike at the LHC, there is no contamination from $pp \to HW, HZ \to Hjj$ type higstrahlung processes at e^-p collider. Further, if we compare $e^-p \to e^-Hj$ with $pp \to Hjj$, we find that due to an asymmetry in the beam type and beam energies, the rapidity difference $\Delta\eta(e,j)$ distribution is shifted towards the left with respect to $\Delta\eta(j,j)$. Also, the Higgs produced in e^-p collisions is always in the forward or backward region while the Higgs produced in pp collisions, due to a symmetric environment, is detected in both forward and backward regions.

In various proposals and studies for e^-p collider, the electron beam energy has been considered in the range of 50-200 GeV [74]. On the other hand, keeping the proposal of FCC-hh [75] in mind, a proton beam with energy as large as 50 TeV can also be taken. In figure 2, we show the dependence of the standard model cross section for possible electron and proton beam energies. The cross sections in these plots are produced in `MadGraph5_aMC@NLO`(MG5) [76] with cuts $p_T(e) > 20\,\text{GeV}$, $p_T(j) > 20\,\text{GeV}$, $|\eta_j| < 4.5$, $|\eta_e| < 2.5$, $\Delta R(e,j) > 0.4$ for NC and $\not{E}_T > 20\,\text{GeV}$, $p_T(j) > 20\,\text{GeV}$, $|\eta_j| < 4.5$ for CC

JHEP10(2022)108

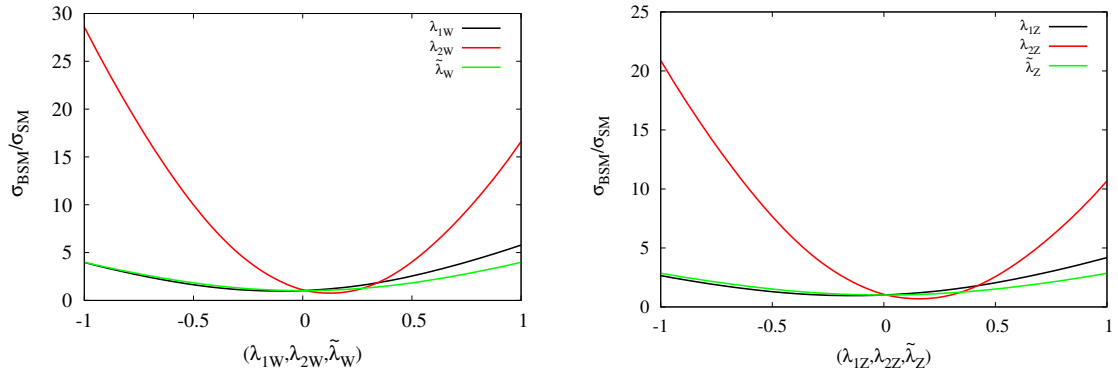

(a) **(b)**

Figure 3. Variation of CC (left) and NC (right) cross sections with respect to the non-trivial BSM parameters.

process. We generated events using the NN23LO1 parton distribution function choosing a common dynamical scale for renormalization and factorization. The default choice of this scale is related to the transverse energy of the final state particles. The BSM model file for madgraph is produced using the FeynRules package [77]. We note that the effect of electron beam energy on the cross section is stronger than that of proton beam energy. For our present study, we choose $E_e = 60\,\text{GeV}$ and $E_p = 7\,\text{TeV}$ which corresponds to a center-of-mass energy of 1.3 TeV. At this energy, the standard model cross sections for CC and NC processes are respectively 88 fb and 16 fb with the unpolarized electron beam. With the -80 % polarized electron beam, the cross sections become 158 fb and 19 fb respectively. The significant change in the CC cross section when using the polarized electron beam is simply related to the fact that the W boson couples to the left-handed fermions only. The PDF and scale uncertainties are about 2.5% and 5% respectively.

In presence of the BSM parameters introduced above, the inclusive or differential cross section, denoted by X, can be written symbolically as

$$X^{\text{BSM}} = X^{\text{SM}} + \sum_i X_i c_i + \sum_{i,j} X_{ij} c_i c_j. \tag{2.1}$$

Here, $c_i = \kappa_V, \lambda_{1V}, \lambda_{2V}, \tilde{\lambda}_V$. Variation of the cross sections with respect to each non-trivial BSM parameter is shown in figure 3 for both CC and NC processes. We can infer that the inclusive cross section is most sensitive to λ_{2V} and least sensitive to $\tilde{\lambda}_V$. Since the vector bosons are connected to massless fermions, terms proportional to $p_i^\mu p_i^\nu (i = 1, 2)$ do not contribute. The parameter λ_{2V}, thus, directly probes the off-shellness of the vector bosons. Also, the variations for +ve and -ve values suggest that the linear term is more relevant in presence of λ_{2V} than in presence of λ_{1V}. Being CP even observable, the cross section does not depend on $\tilde{\lambda}_V$ linearly. The effect of κ_V is standard model-like and the cross sections scale as κ_V^2.

Our study involves both CP-even and CP-odd BSM parameters. It is, therefore, desirable to look for observables which can efficiently distinguish these two types of couplings.

JHEP10(2022)108

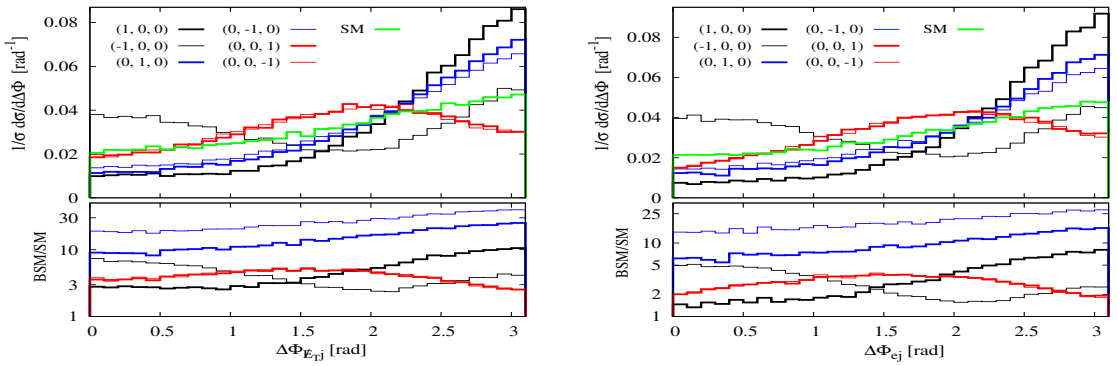

(a) (b)

Figure 4. BSM effects in azimuthal angle distributions for CC (left) and NC (right) processes. The numerical values in the brackets refer to the values of BSM parameters $(\lambda_{1V}, \lambda_{2V}, \tilde{\lambda}_V)$. The lower panel in each plot gives the ratio of BSM and SM predictions.

In the context of Higgs physics, pure CP-odd observables have been proposed in processes with charge-neutral final states at e^+e^- and pp colliders [24, 28]. In ref. [30] it has been shown that $\Delta\phi$ distribution (positive difference of azimuthal angles between $\not{E}_T$ and the jet) is useful in distinguishing CP-even coupling with CP-odd coupling in the CC process. A similar conclusion can be inferred from the VBF study at the LHC presented in [32]. The behaviour of $\Delta\phi$ distributions (normalized by the total cross section) for individual parameters (λ_{1V}, λ_{2V}, and $\tilde{\lambda}_V$) are shown in figure 4 by taking 0, ± 1 as benchmark values of these parameters. The choices of benchmark values are completely ad hoc and these values are taken only to illustrate the individual effect of parameters on $\Delta\phi$ distributions. As expected, the BSM effects are not flat across bins. We note that in both CC and NC processes, $\Delta\phi$ for CP-odd parameter is characteristically different from $\Delta\phi$ for CP-even parameters. Also, the distribution is symmetric for +ve and -ve values of $\tilde{\lambda}_V$. In presence of λ_{1V}, the distribution peaks in opposite direction for +ve and -ve values. Thus $\Delta\phi$ distribution can differentiate between λ_{1V} and λ_{2V} as well.

3 Collider simulation: signal vs background

Considering the dominant decay channel $H \to b\bar{b}$, we identify signal events with missing transverse energy (due to neutrinos), two b jets, and one light jet $j = (u, d, c, s, g)$ in the final state of the CC process. As indicated earlier, the gluon does not enter in the signal process at the leading order. Apart from the QCD-induced irreducible backgrounds from $e^-p \to \nu_e b\bar{b}j$, there are a number of reducible backgrounds coming from; (i) $e^-p \to \nu_e t\bar{b} \to \nu_e b\bar{b}jj$ in which the two jets are misidentified as one jet[2] (ii) $e^-p \to \nu_e jjj$ in which two of the three light jets are mistagged as b jets. Another reducible background comes from $e^-p \to e^- b\bar{b}j$ via photo production ($\gamma^* p \to b\bar{b}j$). In this process, the scattered

[2]We have explicitly checked that other background channels with $\nu_e b\bar{b}jj$ final state are not significant and only 2 events are left after applying the analysis cuts discussed below.

JHEP10(2022)108

electrons are all very close to the beam pipe which do not get registered in the detector giving rise to missing energy signature.

We have generated the signal and background events at the parton level using MG5 with the following selection cuts.

$$p_T(j) > 10 \text{ GeV}; \ \Delta R(b,b), \Delta R(b,j) > 0.4$$

We use the energy smearing function given by,

$$\frac{\sigma_E}{E} = a/\sqrt{E} \oplus b \tag{3.1}$$

to take into account the detector effects. We choose $a = 0.6,\ b = 0.04$ for parton jets, and $a = 0.12,\ b = 0.02$ for electron [74]. After taking into account the smearing effects, we apply $p_T(j),\ p_T(b) > 30\,\text{GeV}$ cuts. To take care of the photo production background, we apply $\not{E}_T$ cut of 25 GeV. As in ref. [72], we find that $\not{E}_T$ cut is indeed very effective in suppressing the photo production background. The two jet background events are ordered in rapidity and we apply a veto on the less forward jet with $p_T > 30\,\text{GeV}$.

Next, we impose $|M(b,\bar{b}) - M_H| < 15\,\text{GeV}$ cut which is effective on all background processes. At this stage, $e^-p \to \nu_e \bar{t} b, \bar{t} \to \bar{b}jj$ is the only relevant background. In order to improve the significance of the signal over backgrounds, we demand that the jet is in the forward region i.e. $1 < |\eta_j| < 5.0$. This reduces the irreducible background considerably. Finally, we apply $M(H,j) > 250\,\text{GeV}$ cut which further reduces the background. Many of these cuts are motivated by the VBF studies performed for the LHC. In our analysis, we use a 60% tagging rate for b jets. We note that the irreducible backgrounds $\nu_e jjj$ are negligible after considering c jet, and light jet mistagging rates as 0.1, and 0.01 respectively. In table 1, we summarize the effect of various cuts on signal and dominant background processes.

In the case of the NC process, all the final state particles can be seen in the detector. The dominant backgrounds mimicking $e^-H(b\bar{b})j$ final state include (i) the irreducible background $e^-p \to e^-b\bar{b}j$ and (ii) reducible background $e^-p \to e^-b\bar{b}jj$. In this case, the generation cuts on particles other than e^- are as before. On the e^- following generation cuts are applied.

$$p_T(e) > 10 \text{ GeV}; \ \Delta R(e,b), \Delta R(e,j) > 0.4$$

The signal significance is very poor due to a very large background at this stage. Selection cuts $p_T(e) > 20\,\text{GeV}$, $p_T(j) > 30\,\text{GeV}$ and $p_T(b) > 30\,\text{GeV}$ reduce dominant backgrounds almost 99% at the cost of losing half of the signal events. These cuts are very effective on the $2j$ background. Further, we impose invariant mass cut $|M(b,\bar{b}) - M_H| < 15\,\text{GeV}$ which reduces the irreducible background significantly. Pseudo-rapidity cuts as given in the table 2 reduce backgrounds and improve the S/B ratio. The final cut of $M(H,j) > 300\,\text{GeV}$ brings down the total background to 16% of the background at the previous stage with an increased S/B ratio of 0.41. We have ignored the contribution from the reducible background $e^-p \to e^-jjj$ as it takes down the S/B from 0.41 to 0.38 which does not have a significant impact on our results. A cut-flow chart for the NC process is presented in table 2.

The cuts discussed for the CC and NC standard model processes are kept fixed for non-zero values of the BSM parameters. We assume that cut efficiencies do not change substantially for reasonable values of BSM parameters.

JHEP10(2022)108

	Generation cuts after smearing	$p_T(j) >$ 30 GeV, $p_T(b) >$ 30 GeV, $\not{E}_T >$ 25GeV	$\lvert M_{b\bar{b}} - m_H \rvert$ < 15 GeV	$1 < \eta_j < 5.0$, $-1 < \eta_b < 4.0$	$M_{Hj} >$ 250 GeV
SM signal	3011	1315	1296	1251	819
$e^- p \to \nu_e b\bar{b} j$	18883	1877	83	60	30
$e^- p \to \nu_e \bar{t} b$, $\bar{t} \to \bar{b} j j$	10985	1597	326	152	38
S/B	0.1	0.4	3.2	5.9	12.0

Table 1. SM signal and background events (at $\mathcal{L} = 100\ fb^{-1}$) with selection cuts for the CC process. Signal to background ratio (S/B) is given in the last row. A tagging efficiency of 60% for b quark is assumed. For -80% polarized electron, the S/B ratio changes to 11.0.

4 Projected constraints on BSM parameters

In order to estimate constraints on anomalous couplings, we perform χ^2 analysis assuming the standard model hypothesis. The analysis is done first at the inclusive level and then using $\Delta\phi$ distribution for each process. For a given BSM parameter c_i, the χ^2 function is given by,

$$\chi^2(c_i) = \sum_{j=1}^{n} \left(\frac{N_j^{\rm BSM}(c_i) - N_j^{\rm SM}}{\Delta N_j} \right)^2 , \tag{4.1}$$

where $N_j^{\rm SM}$ and $N_j^{\rm BSM}$ are the numbers of SM and BSM events in the $j^{\rm th}$ bin of the $\Delta\phi$ distribution after applying all the cuts and efficiencies discussed in the previous section. The uncertainty in the $j^{\rm th}$ bin, ΔN_j includes both statistical and systematic uncertainties. It is given by,

$$\Delta N_j^{\rm SM+Bkg} = \sqrt{N_j^{\rm SM+Bkg} \left(1 + \delta_{sys}^2 N_j^{\rm SM+Bkg}\right)}. \tag{4.2}$$

For our analysis, presented in the next subsections, we choose 5% systematic uncertainty uniformly in all the bins. Typically it is in the range of 2-3%. For more details on this see table 6.1 in [74]. Due to limited statistics at low luminosity, we restrict our analysis to two bins of the $\Delta\phi$ distribution. We choose these two bins symmetrically at

JHEP10(2022)108

	Generation level cuts	$p_T(e) >$ 20 GeV, $p_T(j) >$ 30 GeV, $p_T(b) >$ 30 GeV	$\lvert M_{b\bar{b}} - m_H \rvert \leq 15$ GeV	$\lvert\eta_e\rvert < 2.5$, $2 < \eta_j < 5$, $0.5 < \eta_b < 3$	$M_{Hj} >$ 300 GeV
SM signal	534	274	270	161	76
$e^- p \to e^- b\bar{b} j$	2.75×10^6	1.3×10^4	2425	835	161
$e^- p \to e^- b\bar{b} jj$	6.3×10^5	4218	789	336	24
S/B	0.02×10^{-2}	0.02	0.08	0.14	0.41

Table 2. SM signal and background events (at $\mathcal{L} = 100\ fb^{-1}$) with selection cuts for the `NC` process. Signal to background ratio (S/B) is given in the last row. We have assumed b tagging efficiency of 60%. For -80% polarized electron, the S/B ratio changes to 0.3.

	First Bin			Second Bin		
Couplings	X_{ii} (pb)	X_i (pb)	X_{SM} (pb)	X_{ii} (pb)	X_i (pb)	X_{SM} (pb)
λ_{1W}	0.0140	-0.0052		0.0271	0.0123	
λ_{2W}	0.0737	-0.0218	0.0033	0.1781	-0.0388	0.0049
$\tilde{\lambda}_W$	0.0159	0		0.0176	0	
λ_{1Z}	0.0008	-0.0005		0.0012	0.0008	
λ_{2Z}	0.0067	-0.0022	0.0003	0.0109	-0.0029	0.0004
$\tilde{\lambda}_Z$	0.0009	0		0.0009	0	

Table 3. Coefficients of BSM parameters given in eq. 2.1 for $\Delta\phi$ distribution after applying all the cuts given in tables 1 and 2. Similar coefficients at the total cross section level can be calculated from the two bin information. These numbers are used in the one parameter analysis of section 4.1.

about $\Delta\phi = \pi/2$. Table 3 can be used to obtain the cross section as a function of c_i in each bin after applying the final analysis cuts. The coefficients in the table are extracted by computing the cross sections for $c_i = \pm 1$ on which the cross section dependence is given by eq. 2.1. In the following, we will refer to the analysis based on the total cross section as 1 bin analysis, while the analysis based on $\Delta\phi$ will be referred to as 2 bin analysis.

JHEP10(2022)108

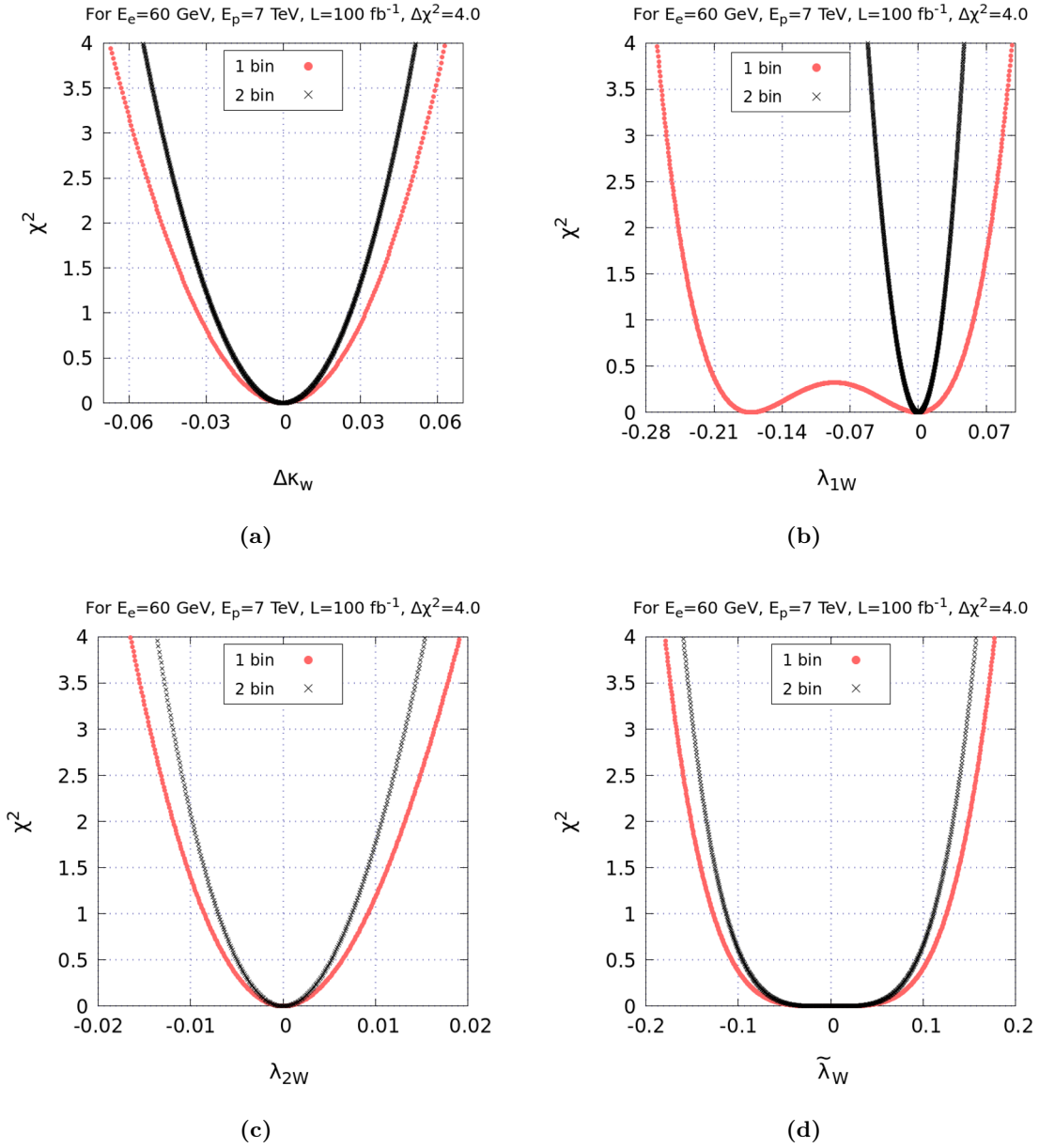

Figure 5. χ^2 distribution for 1 bin (red curve) and 2 bins (black curve) of $\Delta\phi$ distribution in the CC process. In (a), we have defined $\Delta\kappa_W = 1 - \kappa_W$.

4.1 One parameter analysis

First, we consider the case in which only one of the four parameters is taken non-zero at a time. The results of one parameter analysis for an integrated luminosity of 100 fb^{-1} are shown in figures 5 and 6. We find that the 2 bin analysis improves the constraints on all the BSM parameters. From figures 5(a) and 6(a), we note that the constraints on κ_W improve by 26% while constraints on κ_Z improve by 12% in switching from 1 bin to 2 bin analysis. At 95% C.L., the constraints on κ_W and κ_Z are [0.94,1.05] and [0.72,1.22], respectively.

JHEP10(2022)108

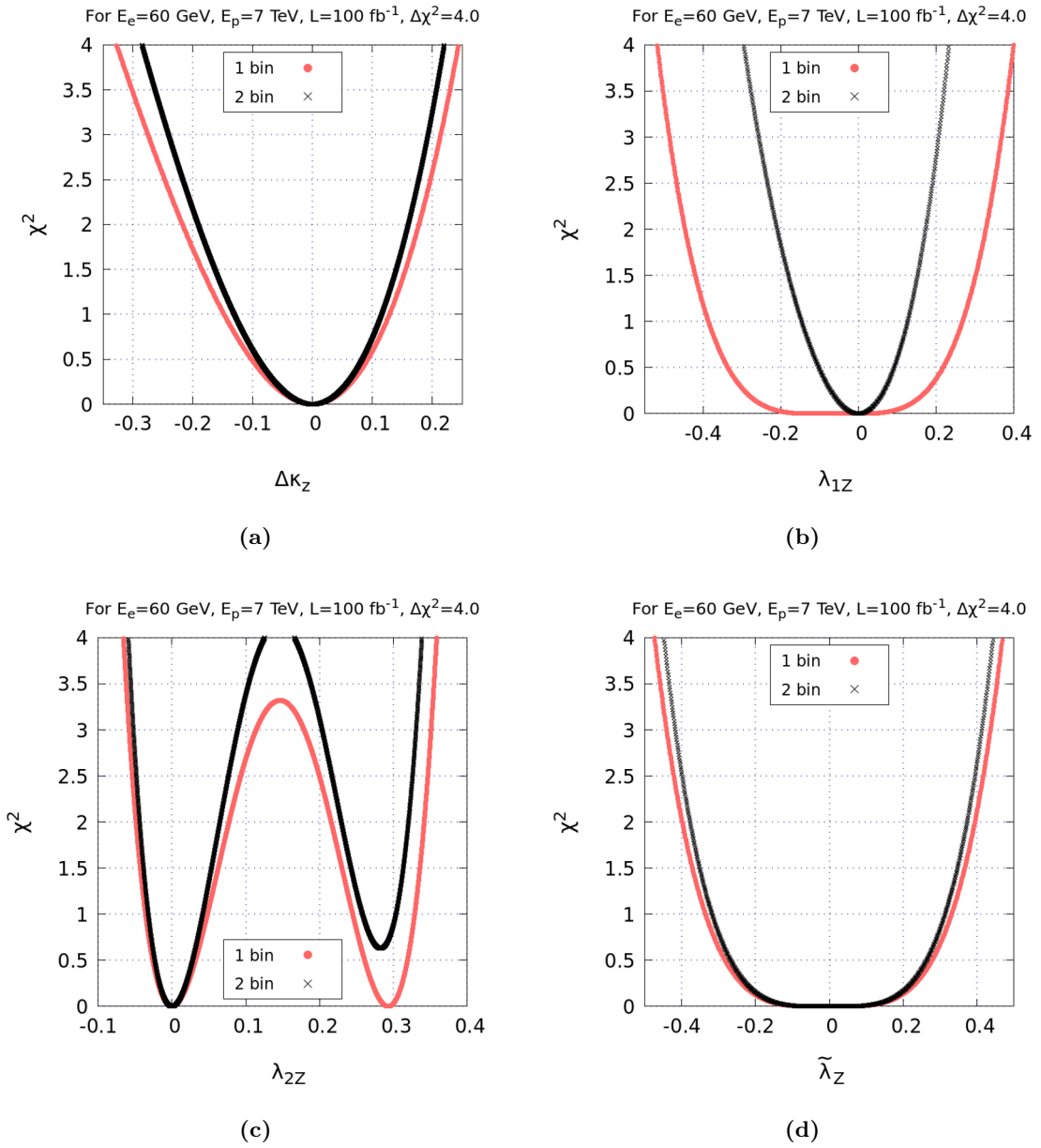

Figure 6. χ^2 distribution for 1 bin (red curve) and 2 bins (black curve) of $\Delta\phi$ distribution in the NC process. In (a), we have defined $\Delta\kappa_Z = 1 - \kappa_Z$.

The fit based on Run-II data (35.9 fb^{-1}) of 13 TeV LHC gives $\kappa_W \in [0.76, 1.34]$ and $\kappa_Z \in [0.75, 1.21]$ at 2σ [78].

In the CC process, the 2 bin analysis leads to significant improvement in constraints on λ_{1W} and λ_{2W} when compared with the 1 bin analysis. For example, at 95% C.L. the allowed region for λ_{1W} in figure 5(b) changes from [-0.26, 0.1] to [-0.05, 0.05] when we change the analysis from 1 bin to 2 bins. Note that the two bin analysis is able to break the degeneracy in χ^2 minimum for λ_{1W} which appears at $\lambda_{1W} = 0$ and $\lambda_{1W} = -0.17$.

JHEP10(2022)108

A similar feature is observed for λ_{2W} in which case the 2nd minimum in χ^2 appears at $\lambda_{2W} = 0.24$. The separation between the two minima is sensitive to the size of the linear term which is much larger in the case of λ_{2W} than in λ_{1W} (see table 3). Since the overall constraints on λ_{2W} are much tighter, in figure 5(c) we have shown the constraints only about $\lambda_{2W} = 0$, the minima chosen by the 2 bin analysis. The allowed regions for λ_{2W} are [-0.016, 0.018] and [-0.013, 0.015] for 1 bin and 2 bin analysis, respectively. Since the cross section depends on $\tilde{\lambda}_W$ quadratically, the two bin analysis leads to only a slight improvement in the constraints as visible in figure 5(d). In going from 1 bin to 2 bin analysis, the allowed region changes from [-0.18, 0.18] to [-0.16, 0.16], accounting for a 10% improvement. We note that these limits are consistent with the limits obtained on λ_{1W} and $\tilde{\lambda}_W$ in ref. [30] with $E_e = 140\,\text{GeV}$ and $E_p = 6.5\,\text{TeV}$. The parameters of HWW have been constrained by studying the double Higgs production at the FCC-he ($E_e = 60\,\text{GeV}$, E_p= 50 TeV), however, those limits are much weaker than ours [34].

In the NC process, constraints on BSM parameters are less stringent as compared to CC process since NC process is background dominated over signal events. Among all BSM parameters, λ_{1Z} is constrained the most as we go from 1 bin to 2 bin analysis. The 2 bin analysis improves the constraint by 41% for this parameter. Unlike in the case of λ_{1W}, the degenerate minima in the 1 bin analysis of λ_{1Z} are not well separated leading to a flat region at the bottom of the plot. The flatness is removed when using the 2 bin information. In the case of λ_{2Z}, the 2 bin analysis breaks the degeneracy, however, a significant region about the second minimum at $\lambda_{2Z} = 0.28$ is still allowed. The allowed region for λ_{2Z} is [-0.06, 0.36] for 1 bin analysis while [-0.06,0.13] $\cup$ [0.17, 0.34] is for 2 bin analysis. Only at a very large luminosity, the second region of the 2 bin analysis can be ruled out. We find that there are no significant changes in the constraints on $\widetilde{\lambda}_Z$ when choosing 2 bin over 1 bin analysis. It is due to the same size of the coefficients of $\widetilde{\lambda}_Z^2$ term in both the bins as given in table 3. The slight improvement in constraints is mainly due to the difference in the errors in the two cases.

We have found that the above constraints improve with an increase in the beam energies of the electron and the proton as expected. However, the effect of increasing electron energy on constraints is more than increasing the proton beam energy. We have also checked that there is no significant improvement in constraints from the NC process if we use -80% polarized electron beam. In the CC process, $\Delta\phi$ distribution increases 1.8 times in each bin for -80% polarized electron beam which leads to about 7-10% improvements in constraints on HWW parameters.

In figure 7, we present one parameter constraints at 95% C.L. as a function of luminosity. We have varied the luminosity from 10 fb^{-1} to 1000 fb^{-1}. All BSM parameters decrease with increasing luminosity and follow the same trend. Changing the luminosity from 10 fb^{-1} to 1000 fb^{-1} improves the constraints by 67%, 40%, 78%, and 42% on κ_W, λ_{1W}, λ_{2W}, and $\widetilde{\lambda}_W$, respectively. In the NC process, unlike κ_Z, λ_{1Z}, and $\widetilde{\lambda}_Z$ parameters, λ_{2Z} has two branches of the allowed region. The allowed regions for κ_Z, λ_{1Z}, λ_{2Z}, and $\widetilde{\lambda}_Z$ shrink by 91%, 74%, 73%, and 55%, respectively as the luminosity is changed from 10 fb^{-1} to 1000 fb^{-1}. Projected constraints for $\mathcal{L} = 1000\,fb^{-1}$ are summarized in table 4. For reference we mention that at 2σ, the expected reach on κ_W and κ_Z are 3.4% (1.6%) and 3.0% (0.8%), respectively at HL-LHC (CLIC: 350 GeV, 1 ab^{-1}) [14, 79]. The current limits

JHEP10(2022)108

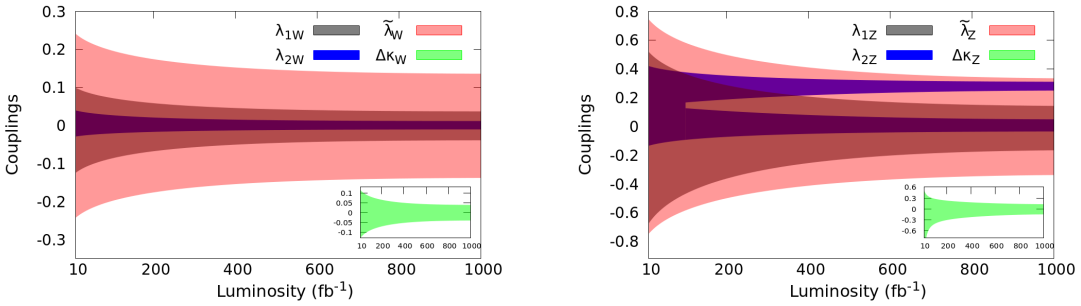

(a) **(b)**

Figure 7. Luminosity vs BSM coupling parameters (a) CC process (b) NC process.

BSM parameter	κ_W κ_Z	λ_{1W} λ_{1Z}	λ_{2W} λ_{2Z}	$\widetilde{\lambda}_W$ $\widetilde{\lambda}_Z$
Constraint	[0.96, 1.04] [0.85, 1.13]	[-0.04, 0.04] [-0.17, 0.14]	[-0.01, 0.01] [-0.04, 0.05] ∪ [0.25, 0.31]	[-0.14, 0.14] [-0.34, 0.34]

Table 4. Projected constraints on BSM parameters with 1000 fb^{-1} integrated luminosity at 95% C.L.

on CP-odd parameters obtained using the Run-II LHC data are $\tilde{\lambda}_Z = \frac{1}{2}\tilde{\lambda}_W \in [-0.21, 0.15]$ at 2σ [80]. The projections at HL-LHC for $\lambda_{1Z}, \lambda_{2Z}$, and $\tilde{\lambda}_Z$ are about 1%, 0.7%, and 12%, respectively [14, 35].

4.2 Two parameter analysis

The results of one parameter analysis discussed above provide the most conservative bound on each BSM parameter. These bounds are useful in a scenario when two out of three nontrivial BSM parameters can be constrained severely using some other observables. In a more general scenario, one would like to know how constraints on a given BSM parameter change in presence of other BSM parameters. For that, we consider the case in which two of the three non-trivial BSM couplings are taken non-zero at a time. In figures 8 and 9, two parameter spaces consistent with the SM hypothesis at 95% CL are shown for the CC and NC processes, respectively. An integrated luminosity of 100 fb^{-1} has been assumed. The plots are obtained by taking $\Delta\chi^2$=6.18 around minima. This value corresponds to 95% C.L. for 2 parameter case [81].

In each figure, we display the effect of using differential distribution in the χ^2 analysis. Two parameter analysis results are consistent with one parameter results. We note that the efficacy of 2 bin analysis over 1 bin analysis is stronger on the parameters of the CC process as compared to those of the NC process. Since λ_{1V} and λ_{2V} are CP-even parameters, the constraints on them are correlated, that is, the coefficient of cross-term in the observable is sufficiently large.

Contour plots for 1 bin analysis in the planes of $(\lambda_{1W}, \lambda_{2W})$ and $(\lambda_{2W}, \widetilde{\lambda}_W)$ are ring-shaped. This is related to the fact that the 1 parameter fit for λ_{2W} using the total cross

JHEP10(2022)108

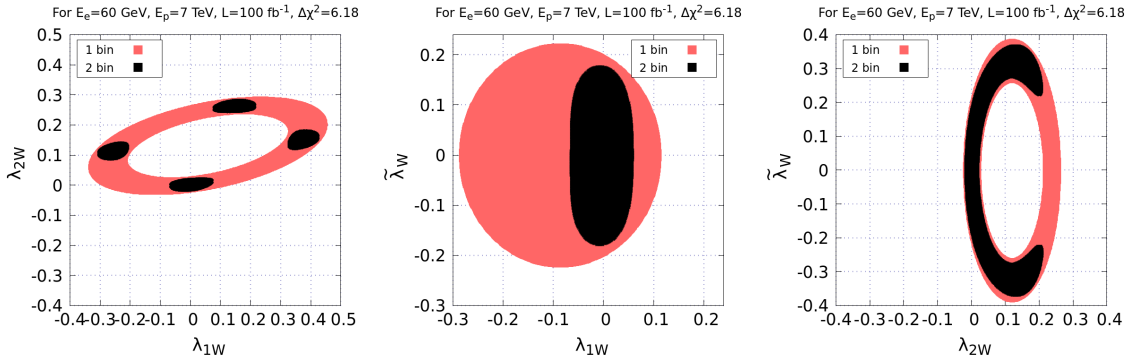

(a) **(b)** **(c)**

Figure 8. Two-dimensional parameter space for HWW BSM parameters at $\mathcal{L} = 100\, fb^{-1}$ using cross section (red) and $\Delta\phi$ distribution (black) as observables.

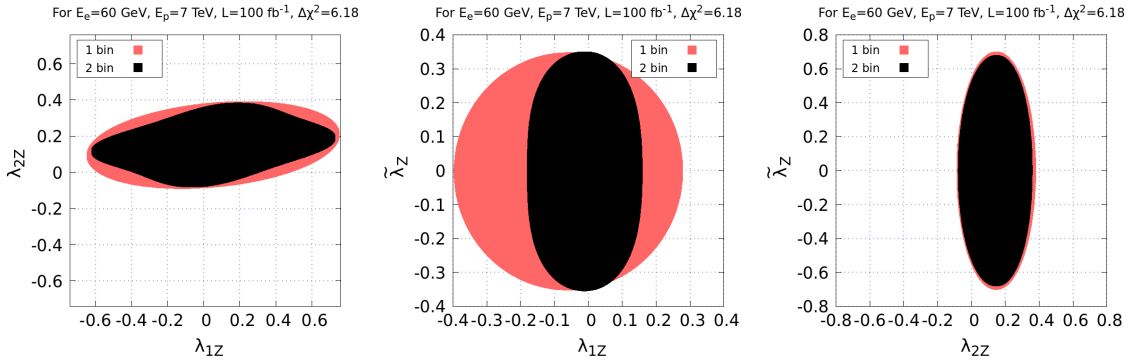

(a) **(b)** **(c)**

Figure 9. Two-dimensional parameter space for HZZ BSM parameters at $\mathcal{L} = 100\, fb^{-1}$ using cross section (red) and $\Delta\phi$ distribution (black) as observables.

section information results in two well-separated allowed regions. This happens for some non-zero values of λ_{1W} and $\tilde{\lambda}_W$ as well. The effect of the 2 bin analysis is most prominent in the $(\lambda_{1W}, \lambda_{2W})$ plane where the allowed region reduces to four disconnected regions in figure 8(a). Depending on the value of λ_{1W}, large values of λ_{2W} such as 0.25 are allowed. It is clear from figure 8(c) that this value, however, is not compatible with any value of $\widetilde{\lambda}_W$ when $\lambda_{1W} = 0$. The region constrained by 1 bin analysis, in the plane of $(\lambda_{1W}, \widetilde{\lambda}_W)$ is almost a circular disc which, when using 2 bin analysis, shrinks into an elliptical region with the major axis about $\lambda_{1W} = 0$.

In the NC process, parameter space in the plane of $(\lambda_{1Z}, \widetilde{\lambda}_Z)$ shows significant improvement when 2 bin analysis is used. The constraints in other cases change only marginally. Substantially large data would be required in order to constrain the two parameter regions of the NC process.

JHEP10(2022)108

5 Conclusions

We have studied the CC and NC processes for single Higgs production at an $e^- p$ collider with $E_e = 60\,\text{GeV}$ and $E_p = 7000\,\text{GeV}$. The effects of the most general HVV vertices, which are relevant to these processes, on the total cross sections and the $\Delta\phi$ distributions have been studied. We find that using $\Delta\phi$ distribution in the analysis over the total cross section leads to stronger bounds on the BSM parameters. Constraints obtained for CP-even parameters are tighter than those on CP-odd parameters.

We have obtained the constraints in two scenarios; (i) only one BSM parameter is non-zero at a time and (ii) two BSM parameters are non-zero at a time. Assuming the SM hypothesis, the one parameter constraints lie in the range of 1-15% for HWW parameters, and 5-34% for HZZ parameters with 1000 fb^{-1} data at 95% C.L. These constraints change considerably when some other BSM parameters are present. In the case of two parameter analysis, the $\Delta\phi$ distribution is most effective in constraining $(\lambda_{1W}, \lambda_{2W})$, $(\lambda_{1W}, \tilde{\lambda}_W)$, $(\lambda_{2W}, \tilde{\lambda}_W)$ and $(\lambda_{1Z}, \tilde{\lambda}_Z)$ parameter regions. The projected constraints on HWW parameters κ_W and $\tilde{\lambda}_W$, from our analysis of the CC process, are compatible with the expected reach at the future colliders HL-LHC and CLIC. However, the constraints on HZZ parameters from the study of the NC process are weaker than the projections at future colliders.

Although we have limited our study to one parameter and two parameter fits, a multi-parameter analysis taking all the BSM parameters non-zero is needed to understand the direction of new physics more precisely.

Acknowledgments

We would like to acknowledge fruitful discussions with Rafiqul Rahaman on the signal-background analysis. We thank Mukesh Kumar for various discussions and his participation in the initial stages of the project. Special thanks to Olivier Mattelaer for his help with the MG5 package. PS would like to acknowledge financial support from IISER Mohali for this work.

References

[1] S.L. Glashow, *Partial symmetries of weak interactions*, *Nucl. Phys.* **22** (1961) 579 [INSPIRE].

[2] F. Englert and R. Brout, *Broken symmetry and the mass of gauge vector mesons*, *Phys. Rev. Lett.* **13** (1964) 321 [INSPIRE].

[3] P.W. Higgs, *Broken symmetries, massless particles and gauge fields*, *Phys. Lett.* **12** (1964) 132 [INSPIRE].

[4] P.W. Higgs, *Broken symmetries and the masses of gauge bosons*, *Phys. Rev. Lett.* **13** (1964) 508 [INSPIRE].

JHEP10(2022)108

[5] G.S. Guralnik, C.R. Hagen and T.W.B. Kibble, *Global conservation laws and massless particles*, *Phys. Rev. Lett.* **13** (1964) 585 [INSPIRE].

[6] S. Weinberg, *A model of leptons*, *Phys. Rev. Lett.* **19** (1967) 1264 [INSPIRE].

[7] A. Salam, *Weak and electromagnetic interactions*, in *Proceedings of the eighth Nobel symposium*, (1968) [*Conf. Proc. C* **680519** (1968) 367] [INSPIRE].

[8] ATLAS collaboration, *Observation of a new particle in the search for the Standard Model Higgs boson with the ATLAS detector at the LHC*, *Phys. Lett. B* **716** (2012) 1 [arXiv:1207.7214] [INSPIRE].

[9] CMS collaboration, *Observation of a new boson at a mass of* 125 *GeV with the CMS experiment at the LHC*, *Phys. Lett. B* **716** (2012) 30 [arXiv:1207.7235] [INSPIRE].

[10] CMS collaboration, *Observation of a new boson with mass near* 125 *GeV in pp collisions at* $\sqrt{s} = 7$ *and* 8 *TeV*, *JHEP* **06** (2013) 081 [arXiv:1303.4571] [INSPIRE].

[11] J. de Blas et al., *Higgs boson studies at future particle colliders*, *JHEP* **01** (2020) 139 [arXiv:1905.03764] [INSPIRE].

[12] ATLAS collaboration, *Measurements of the Higgs boson production and decay rates and constraints on its couplings from a combined ATLAS and CMS analysis of the LHC pp collision data at* $\sqrt{s} = 7$ *and* 8 *TeV*, Tech. Rep. ATLAS-CONF-2015-044, CERN, Geneva, Switzerland (2015).

[13] CMS collaboration, *Measurements of the Higgs boson production and decay rates and constraints on its couplings from a combined ATLAS and CMS analysis of the LHC pp collision data at* $\sqrt{s} = 7$ *and* 8 *TeV*, Tech. Rep. CMS-PAS-HIG-15-002, CERN, Geneva, Switzerland (2015).

[14] M. Cepeda et al., *Report from working group* 2*: Higgs physics at the HL-LHC and HE-LHC*, *CERN Yellow Rep. Monogr.* **7** (2019) 221 [arXiv:1902.00134] [INSPIRE].

[15] LHC Higgs Cross Section Working Group collaboration, *Handbook of LHC Higgs cross sections:* 4*. Deciphering the nature of the Higgs sector*, arXiv:1610.07922 [INSPIRE].

[16] W. Buchmüller and D. Wyler, *Effective Lagrangian analysis of new interactions and flavor conservation*, *Nucl. Phys. B* **268** (1986) 621 [INSPIRE].

[17] G.F. Giudice, C. Grojean, A. Pomarol and R. Rattazzi, *The strongly-interacting light Higgs*, *JHEP* **06** (2007) 045 [hep-ph/0703164] [INSPIRE].

[18] B. Grzadkowski, M. Iskrzynski, M. Misiak and J. Rosiek, *Dimension-six terms in the Standard Model Lagrangian*, *JHEP* **10** (2010) 085 [arXiv:1008.4884] [INSPIRE].

[19] A. Alloul, B. Fuks and V. Sanz, *Phenomenology of the Higgs effective lagrangian via FeynRules*, *JHEP* **04** (2014) 110 [arXiv:1310.5150] [INSPIRE].

[20] A. Falkowski and F. Riva, *Model-independent precision constraints on dimension-*6 *operators*, *JHEP* **02** (2015) 039 [arXiv:1411.0669] [INSPIRE].

[21] I. Brivio and M. Trott, *The Standard Model as an effective field theory*, *Phys. Rept.* **793** (2019) 1 [arXiv:1706.08945] [INSPIRE].

[22] K. Hagiwara and M.L. Stong, *Probing the scalar sector in* $e^+e^- \to f\bar{f}H$, *Z. Phys. C* **62** (1994) 99 [hep-ph/9309248] [INSPIRE].

JHEP10(2022)108

[23] K. Hagiwara, S. Ishihara, J. Kamoshita and B.A. Kniehl, *Prospects of measuring general Higgs couplings at e^+e^- linear colliders*, *Eur. Phys. J. C* **14** (2000) 457 [hep-ph/0002043] [INSPIRE].

[24] T. Han and J. Jiang, *CP violating ZZH coupling at e^+e^- linear colliders*, *Phys. Rev. D* **63** (2001) 096007 [hep-ph/0011271] [INSPIRE].

[25] T. Han, Y.-P. Kuang and B. Zhang, *Anomalous gauge couplings of the Higgs boson at high energy photon colliders*, *Phys. Rev. D* **73** (2006) 055010 [hep-ph/0512193] [INSPIRE].

[26] S.S. Biswal, D. Choudhury, R.M. Godbole and Mamta, *Role of polarization in probing anomalous gauge interactions of the Higgs boson*, *Phys. Rev. D* **79** (2009) 035012 [arXiv:0809.0202] [INSPIRE].

[27] S. Dutta, K. Hagiwara and Y. Matsumoto, *Measuring the Higgs-vector boson couplings at linear e^+e^- collider*, *Phys. Rev. D* **78** (2008) 115016 [arXiv:0808.0477] [INSPIRE].

[28] N.D. Christensen, T. Han and Y. Li, *Testing CP-violation in ZZH interactions at the LHC*, *Phys. Lett. B* **693** (2010) 28 [arXiv:1005.5393] [INSPIRE].

[29] N. Desai, D.K. Ghosh and B. Mukhopadhyaya, *CP-violating HWW couplings at the Large Hadron Collider*, *Phys. Rev. D* **83** (2011) 113004 [arXiv:1104.3327] [INSPIRE].

[30] S.S. Biswal, R.M. Godbole, B. Mellado and S. Raychaudhuri, *Azimuthal angle probe of anomalous HWW couplings at a high energy ep collider*, *Phys. Rev. Lett.* **109** (2012) 261801 [arXiv:1203.6285] [INSPIRE].

[31] I.T. Cakir, O. Cakir, A. Senol and A.T. Tasci, *Probing anomalous HZZ couplings at the LHeC*, *Mod. Phys. Lett. A* **28** (2013) 1350142 [arXiv:1304.3616] [INSPIRE].

[32] F. Maltoni, K. Mawatari and M. Zaro, *Higgs characterisation via vector-boson fusion and associated production: NLO and parton-shower effects*, *Eur. Phys. J. C* **74** (2014) 2710 [arXiv:1311.1829] [INSPIRE].

[33] I. Anderson et al., *Constraining anomalous HVV interactions at proton and lepton colliders*, *Phys. Rev. D* **89** (2014) 035007 [arXiv:1309.4819] [INSPIRE].

[34] M. Kumar et al., *Probing anomalous couplings using di-Higgs production in electron-proton collisions*, *Phys. Lett. B* **764** (2017) 247 [arXiv:1509.04016] [INSPIRE].

[35] S. Boselli, C.M. Carloni Calame, G. Montagna, O. Nicrosini, F. Piccinini and A. Shivaji, *Higgs decay into four charged leptons in the presence of dimension-six operators*, *JHEP* **01** (2018) 096 [arXiv:1703.06667] [INSPIRE].

[36] J. Nakamura, *Polarisations of the Z and W bosons in the processes $pp \to ZH$ and $pp \to W^{\pm}H$*, *JHEP* **08** (2017) 008 [arXiv:1706.01816] [INSPIRE].

[37] H.-D. Li, C.-D. Lü and L.-Y. Shan, *Sensitivity study of anomalous HZZ couplings at a future Higgs factory*, *Chin. Phys. C* **43** (2019) 103001 [arXiv:1901.10218] [INSPIRE].

[38] B. Şahin, *Search for the anomalous ZZH couplings at the CLIC*, *Mod. Phys. Lett. A* **34** (2019) 1950299 [INSPIRE].

[39] S. Banerjee, R.S. Gupta, J.Y. Reiness and M. Spannowsky, *Resolving the tensor structure of the Higgs coupling to Z-bosons via Higgs-strahlung*, *Phys. Rev. D* **100** (2019) 115004 [arXiv:1905.02728] [INSPIRE].

JHEP10(2022)108

[40] K. Rao, S.D. Rindani and P. Sarmah, *Probing anomalous gauge-Higgs couplings using Z boson polarization at e^+e^- colliders*, *Nucl. Phys. B* **950** (2020) 114840 [arXiv:1904.06663] [INSPIRE].

[41] T. Han, D. Liu, I. Low and X. Wang, *Electroweak couplings of the Higgs boson at a multi-TeV muon collider*, *Phys. Rev. D* **103** (2021) 013002 [arXiv:2008.12204] [INSPIRE].

[42] S. Banerjee, R.S. Gupta, O. Ochoa-Valeriano, M. Spannowsky and E. Venturini, *A fully differential SMEFT analysis of the golden channel using the method of moments*, *JHEP* **06** (2021) 031 [arXiv:2012.11631] [INSPIRE].

[43] W. Bizoń, F. Caola, K. Melnikov and R. Röntsch, *Anomalous couplings in associated VH production with Higgs boson decay to massive b quarks at NNLO in QCD*, *Phys. Rev. D* **105** (2022) 014023 [arXiv:2106.06328] [INSPIRE].

[44] B. Yan, *Determining Higgs boson width at electron-positron colliders*, *Phys. Lett. B* **822** (2021) 136709 [arXiv:2105.04530] [INSPIRE].

[45] K. Rao, S.D. Rindani, P. Sarmah and B. Singh, *Polarized Z cross sections in Higgsstrahlung for the determination of anomalous ZZH couplings*, arXiv:2202.10215 [INSPIRE].

[46] K. Asteriadis, F. Caola, K. Melnikov and R. Röntsch, *Anomalous Higgs boson couplings in weak boson fusion production at NNLO in QCD*, arXiv:2206.14630 [INSPIRE].

[47] A. Senol, *Anomalous Higgs couplings at the LHeC*, *Nucl. Phys. B* **873** (2013) 293 [arXiv:1212.6869] [INSPIRE].

[48] S. Banerjee, S. Mukhopadhyay and B. Mukhopadhyaya, *Higher dimensional operators and the LHC Higgs data: the role of modified kinematics*, *Phys. Rev. D* **89** (2014) 053010 [arXiv:1308.4860] [INSPIRE].

[49] N. Craig, M. Farina, M. McCullough and M. Perelstein, *Precision Higgsstrahlung as a probe of new physics*, *JHEP* **03** (2015) 146 [arXiv:1411.0676] [INSPIRE].

[50] G. Amar et al., *Exploration of the tensor structure of the Higgs boson coupling to weak bosons in e^+e^- collisions*, *JHEP* **02** (2015) 128 [arXiv:1405.3957] [INSPIRE].

[51] C. Englert and M. Spannowsky, *Effective theories and measurements at colliders*, *Phys. Lett. B* **740** (2015) 8 [arXiv:1408.5147] [INSPIRE].

[52] J. Ellis, V. Sanz and T. You, *Complete Higgs sector constraints on dimension-6 operators*, *JHEP* **07** (2014) 036 [arXiv:1404.3667] [INSPIRE].

[53] B. Mellado, L. March and X. Ruan, *Probing new physics in the Higgs sector with effective field theories at the Large Hadron Collider*, in 60^{th} *annual conference of the South African institute of physics*, (2015), p. 210.

[54] S. Banerjee, T. Mandal, B. Mellado and B. Mukhopadhyaya, *Cornering dimension-6 HVV interactions at high luminosity LHC: the role of event ratios*, *JHEP* **09** (2015) 057 [arXiv:1505.00226] [INSPIRE].

[55] S. Dwivedi, D.K. Ghosh, B. Mukhopadhyaya and A. Shivaji, *Constraints on CP-violating gauge-Higgs operators*, *Phys. Rev. D* **92** (2015) 095015 [arXiv:1505.05844] [INSPIRE].

[56] C. Englert, R. Kogler, H. Schulz and M. Spannowsky, *Higgs coupling measurements at the LHC*, *Eur. Phys. J. C* **76** (2016) 393 [arXiv:1511.05170] [INSPIRE].

[57] N. Craig, J. Gu, Z. Liu and K. Wang, *Beyond Higgs couplings: probing the Higgs with angular observables at future e^+e^- colliders*, *JHEP* **03** (2016) 050 [arXiv:1512.06877] [INSPIRE].

JHEP10(2022)108

[58] S. Dwivedi, D.K. Ghosh, B. Mukhopadhyaya and A. Shivaji, *Distinguishing CP-odd couplings of the Higgs boson to weak boson pairs*, *Phys. Rev. D* **93** (2016) 115039 [arXiv:1603.06195] [INSPIRE].

[59] F. Ferreira, B. Fuks, V. Sanz and D. Sengupta, *Probing CP-violating Higgs and gauge-boson couplings in the Standard Model effective field theory*, *Eur. Phys. J. C* **77** (2017) 675 [arXiv:1612.01808] [INSPIRE].

[60] C. Degrande, B. Fuks, K. Mawatari, K. Mimasu and V. Sanz, *Electroweak Higgs boson production in the Standard Model effective field theory beyond leading order in QCD*, *Eur. Phys. J. C* **77** (2017) 262 [arXiv:1609.04833] [INSPIRE].

[61] H. Denizli and A. Senol, *Constraints on Higgs effective couplings in $H\nu\bar{\nu}$ production of CLIC at* 380 *GeV*, *Adv. High Energy Phys.* **2018** (2018) 1627051 [arXiv:1707.03890] [INSPIRE].

[62] H. Khanpour and M. Mohammadi Najafabadi, *Constraining Higgs boson effective couplings at electron-positron colliders*, *Phys. Rev. D* **95** (2017) 055026 [arXiv:1702.00951] [INSPIRE].

[63] H. Hesari, H. Khanpour and M. Mohammadi Najafabadi, *Study of Higgs effective couplings at electron-proton colliders*, *Phys. Rev. D* **97** (2018) 095041 [arXiv:1805.04697] [INSPIRE].

[64] S. Banerjee, C. Englert, R.S. Gupta and M. Spannowsky, *Probing electroweak precision physics via boosted Higgs-strahlung at the LHC*, *Phys. Rev. D* **98** (2018) 095012 [arXiv:1807.01796] [INSPIRE].

[65] O. Karadeniz, A. Senol, K.Y. Oyulmaz and H. Denizli, *CP-violating Higgs-gauge boson couplings in $H\nu\bar{\nu}$ production at three energy stages of CLIC*, *Eur. Phys. J. C* **80** (2020) 229 [arXiv:1909.08032] [INSPIRE].

[66] V. Cirigliano, A. Crivellin, W. Dekens, J. de Vries, M. Hoferichter and E. Mereghetti, *CP violation in Higgs-gauge interactions: from tabletop experiments to the LHC*, *Phys. Rev. Lett.* **123** (2019) 051801 [arXiv:1903.03625] [INSPIRE].

[67] F.F. Freitas, C.K. Khosa and V. Sanz, *Exploring the Standard Model EFT in VH production with machine learning*, *Phys. Rev. D* **100** (2019) 035040 [arXiv:1902.05803] [INSPIRE].

[68] B. Henning, D.M. Lombardo and F. Riva, *Improved BSM sensitivity in diboson processes at linear colliders*, *Eur. Phys. J. C* **80** (2020) 220 [arXiv:1909.01937] [INSPIRE].

[69] T. Biswas, A. Datta and B. Mukhopadhyaya, *Following the trail of new physics via the vector boson fusion Higgs boson signal at the Large Hadron Collider*, *Phys. Rev. D* **105** (2022) 055028 [arXiv:2107.05503] [INSPIRE].

[70] LHeC Study Group collaboration, *A Large Hadron electron Collider at CERN: report on the physics and design concepts for machine and detector*, *J. Phys. G* **39** (2012) 075001 [arXiv:1206.2913] [INSPIRE].

[71] O. Bruening and M. Klein, *The Large Hadron electron Collider*, *Mod. Phys. Lett. A* **28** (2013) 1330011 [arXiv:1305.2090] [INSPIRE].

[72] T. Han and B. Mellado, *Higgs boson searches and the $Hb\bar{b}$ coupling at the LHeC*, *Phys. Rev. D* **82** (2010) 016009 [arXiv:0909.2460] [INSPIRE].

[73] R. Contino, M. Ghezzi, C. Grojean, M. Muhlleitner and M. Spira, *Effective Lagrangian for a light Higgs-like scalar*, *JHEP* **07** (2013) 035 [arXiv:1303.3876] [INSPIRE].

[74] LHeC and FCC-he Study Group collaborations, *The Large Hadron-electron Collider at the HL-LHC*, *J. Phys. G* **48** (2021) 110501 [arXiv:2007.14491] [INSPIRE].

JHEP10(2022)108

[75] M. Benedikt et al., *Future Circular Hadron Collider FCC-hh: overview and status*, arXiv:2203.07804 [INSPIRE].

[76] J. Alwall et al., *The automated computation of tree-level and next-to-leading order differential cross sections, and their matching to parton shower simulations*, *JHEP* **07** (2014) 079 [arXiv:1405.0301] [INSPIRE].

[77] A. Alloul, N.D. Christensen, C. Degrande, C. Duhr and B. Fuks, *FeynRules* 2.0 — *a complete toolbox for tree-level phenomenology*, *Comput. Phys. Commun.* **185** (2014) 2250 [arXiv:1310.1921] [INSPIRE].

[78] CMS collaboration, *Combined measurements of Higgs boson couplings in proton-proton collisions at* $\sqrt{s} = 13$ *TeV*, *Eur. Phys. J. C* **79** (2019) 421 [arXiv:1809.10733] [INSPIRE].

[79] A. Robson and P. Roloff, *Updated CLIC luminosity staging baseline and Higgs coupling prospects*, arXiv:1812.01644 [INSPIRE].

[80] ATLAS collaboration, *Test of CP invariance in vector-boson fusion production of the Higgs boson in the* $H \to \tau\tau$ *channel in proton-proton collisions at* $\sqrt{s} = 13$ *TeV with the ATLAS detector*, *Phys. Lett. B* **805** (2020) 135426 [arXiv:2002.05315] [INSPIRE].

[81] Particle Data Group collaboration, *Review of particle physics*, *PTEP* **2022** (2022) 083C01 [INSPIRE].

JHEP10(2022)108